Silver/Graphene Nanocomposites as Catalysts for the Reduction of *p*-Nitrophenol to *p*-Aminophenol: Materials Preparation and Reaction Kinetics Studies

Jiangyong Liu,[1,2] Chenxin Ran,[3] Yuan Pu,[1]* Jie-Xin Wang,[1] Dan Wang[1,4]* and Jian-Feng Chen[1,4]

1. *Beijing Advanced Innovation Center for Soft Matter Science and Engineering, State Key Laboratory of Organic-Inorganic Composites, Beijing University of Chemical Technology, Beijing 100029, China*
2. *College of Chemistry and Chemical Engineering, Yangzhou University, Yangzhou, Jiangsu 225002, China*
3. *International Center for Dielectric Research, Xi'an Jiaotong University, Xi'an 710049, China*
4. *Research Centre of the Ministry of Education for High Gravity Engineering and Technology, Beijing University of Chemical Technology, Beijing 100029, China*

Ag/graphene nanocomposites have been demonstrated to be promising catalysts for hydrogenation reduction of *p*-nitrophenol (*p*-NP) to *p*-aminophenol (*p*-AP). Herein, we reported the synthesis of graphene-supported silver nanoparticles (Ag/G) using one-step and stabilizer-free process. The obtained Ag/G nanocomposites were demonstrated to be efficient catalysts for the reduction of *p*-NP to *p*-AP. The reaction kinetics of the catalytic reduction, including the effects of catalyst concentrations and temperatures are reported. These results are of significant values for the scale-up of using Ag/graphene catalysts for hydrogenation reduction.

Keywords: catalysis, silver nanoparticle, graphene oxide, nanocomposites, *p*-nitrophenol

INTRODUCTION

p-Nitrophenol (*p*-NP), a ubiquitous organic contaminant in the industrial wastewater, is the raw material for the synthesis of *p*-aminophenol (*p*-AP), which is an important intermediate for the production of various medicines, such as paracetamol, phenacetin, and acetanilide.[1,2] In addition, *p*-AP can be used as a dyeing agent, a corrosion inhibitor in paints, a photographic developer, and also an anticorrosion-lubricating agent in fuels for two-cycle engines.[3] Therefore, great attention has been paid to the catalytic reduction of *p*-NP to *p*-AP.[4–6] Various catalysts of metals and metal alloys, such as Au,[7] Pd,[8] Ag,[9] Pt, [10] PtAu,[11] AuPd,[12] and PtPdBi,[13] have shown excellent performance for the catalytic reduction of *p*-NP to *p*-AP. The high surface area, good stability, and abundant surface functional groups of graphene oxides (GO) offer opportunities for further chemical modifications, especially for the anchoring of metals, metal oxides, and other metal-containing composites.[14–19] Previous studies have shown that GO are perfect supports for various metal nanoparticles, and many attempts have been made to prepare GO or RGO hybrids by incorporating metal nanoparticles for the enhancement of certain properties.[20] Silver/graphene composites materials have attracted considerable attention due to the good performance and low cost of Ag, compared with Au, Pt, and Pd.[21–24] The knowledge of the reaction kinetics of the catalytic reaction is important for scale-up applications. However, as far as we are aware, the reaction kinetics studies of the reduction of *p*-nitrophenol to *p*-aminophenol by using Ag/graphene nanocomposites as catalysts are rarely reported.

In this paper, we reported the synthesis of graphene supported silver nanoparticles (Ag/G) using a one-step and stabilizer-free process. The obtained Ag/G nanocomposites were demonstrated to be efficient catalysts for the reduction of *p*-NP to *p*-AP. The reaction kinetics of the catalytic reduction, including the effects of catalyst concentrations and temperatures, are reported. These results are of significant value for the scale-up of the use of Ag/graphene catalysts for hydrogenation reduction.

MATERIALS AND METHODS

Synthesis of GO Nanosheets

The chemically exfoliated graphene oxide used in this work was prepared according to the modified Hummers' method.[25,26] All the reagents were used as received without further purification. In a typical experiment, 2.0 g natural graphite powder (0.99 g/g, 300 mesh, Alfa Aesar) was added to 70 mL sulphuric acid (0.95–0.98 g/g, Sigma-Aldrich, USA) in a flask under vigorous agitation, followed by the addition of 2.0 g sodium nitrate (0.99 g/g, Sigma-Aldrich, USA) at room temperature. The mixture solution was then cooled down to 0 °C in an ice bath. Thereafter, 8.0 g potassium permanganate (0.99 g/g, Sigma-Aldrich, USA) was slowly added into the mixture. The rate of addition was carefully controlled to keep the reaction temperature lower than 20 °C. The mixture was stirred for 2 h at 35 °C. After that, 100 mL of deionized (DI) water was slowly

* *Authors to whom correspondence may be addressed.*
E-mail address: puyuan@mail.buct.edu.cn (Y. Pu); wangdan@mail.buct.edu.cn (D. Wang)
Can. J. Chem. Eng. 95:1297–1304, 2017

DOI 10.1002/cjce.22774
Published online 8 February 2017 in Wiley Online Library (wileyonlinelibrary.com).

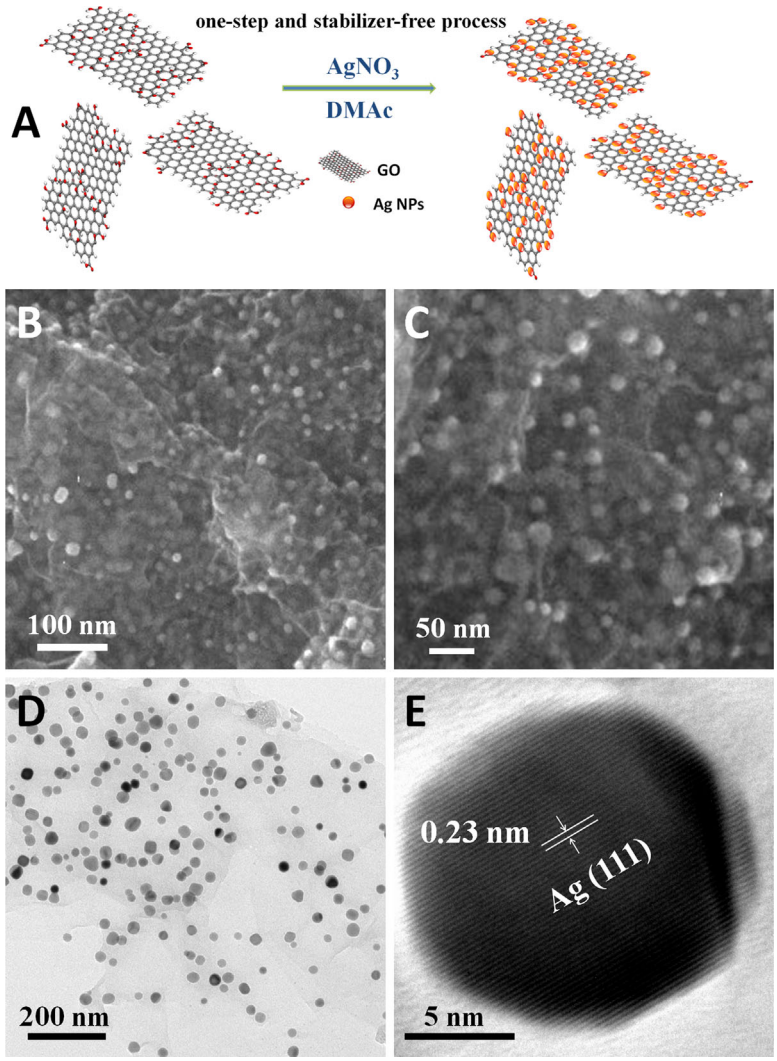

Figure 1. (A) A scheme showing the preparation of Ag/G; (B) SEM images of rGO; (C) SEM images of Ag/G; (D) TEM image of Ag/G; and (E) HR-TEM image of the Ag phase.

added into the mixture. Then the mixture was stirred for 1 h at 98 °C. Upon completion of the reaction, 26 mL of H_2O_2 (0.3 g/g in water, Sigma-Aldrich, USA) was added into the reaction vessel. Finally, the mixture was washed by rinsing and centrifugation with 0.1 g/g HCl (Sigma-Aldrich, USA) and then with DI water several times. The final product was dried under vacuum at 40 °C for 30 h.

Synthesis of Ag/G Nanocomposites

The chemical exfoliation of the obtained GO powder (0.5 mg/mL, 40 mL) was carried out in an ultrasonic bath. In a typical synthesis, Ag/G was prepared by an efficient one-step and stabilizer-free process.[27] After ultrasonication, 40 mL dimethylacetamide (abbreviated DMAc, 0.998 g/g, Sigma-Aldrich, USA)

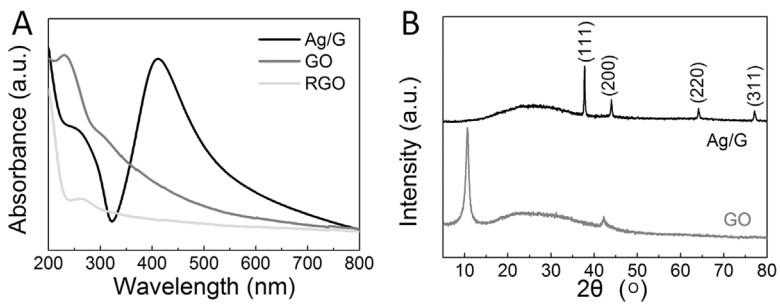

Figure 2. (A) Absorption spectra of GO, rGO, and Ag/G; (B) XRD patterns of GO and Ag/G.

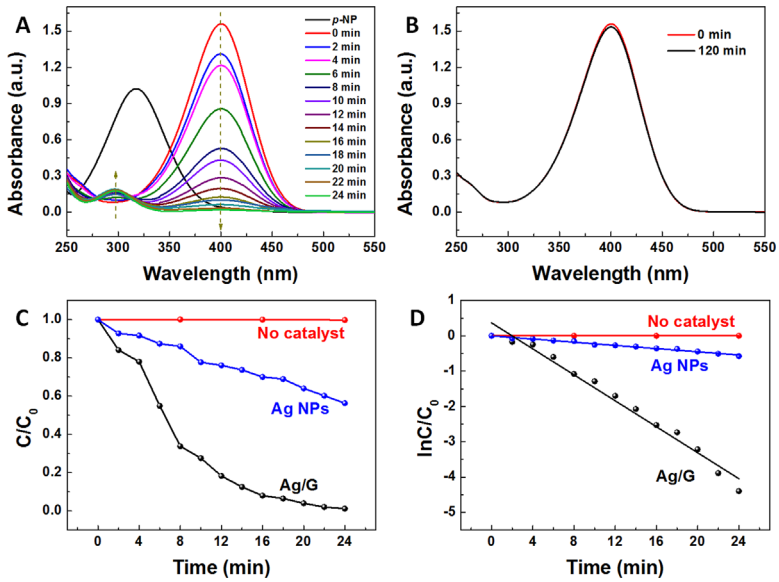

Figure 3. The evolution of UV-vis absorption spectra during the reduction of *p*-NP with Ag/G-s2 as the catalyst (A) and in the absence of catalyst (B); (C and D) C/C_0 and $\ln(C/C_0)$ versus reaction time for the reduction of *p*-NP.

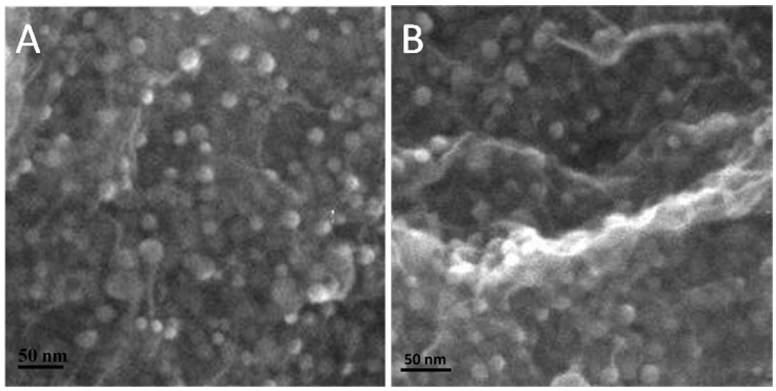

Figure 4. SEM image of Ag/G before (A) and after (B) the reaction.

was added into GO aqueous dispersion, and mixed under vigorous stirring for 15 min at room temperature. Thereafter, 2.0 g of $AgNO_3$ (0.999 999 g/g, Sigma-Aldrich, USA) aqueous solution (0.1 g/g) was added dropwise into the above mixture

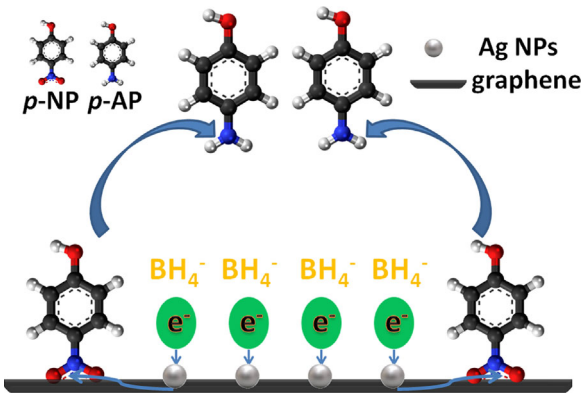

Figure 5. Schematic illustration of the postulate mechanism for the catalytic reduction of *p*-NP with Ag/G as the catalyst.

and allowed for continuous stirring for 0.5 h. Subsequently, the reaction was performed at 150 °C in an oil bath under continuous stirring for 8 h. Finally, the obtained sample was washed thoroughly with DI water, and then filtered through a 0.22 μm Millipore filter, followed by drying under vacuum at 60 °C for 12 h. For a better comparison, bare reduced graphene oxide (rGO) and pure Ag nanoparticles were also prepared with the same process of Ag/G except that only $AgNO_3$ or GO was added.

Characterization of the Nanomaterials

The powder X-ray diffraction patterns (XRD) were recorded within the 2θ range of 5–80° on a Miniflex Desktop X-ray Diffractometer. The UV-vis absorption spectra of the samples were obtained with a spectrophotometer (JASCO V–670 EX, Japan). Thermogravimetric analysis (TGA) was performed on a TA instrument (Q50) with a heating rate of 10 °C/min. The morphology of the samples was investigated with a scanning electron microscope (SEM) (Tescan Vega3). The transmission electron microscopy (TEM) images were obtained on a JEOL JEM-3010 microscope.

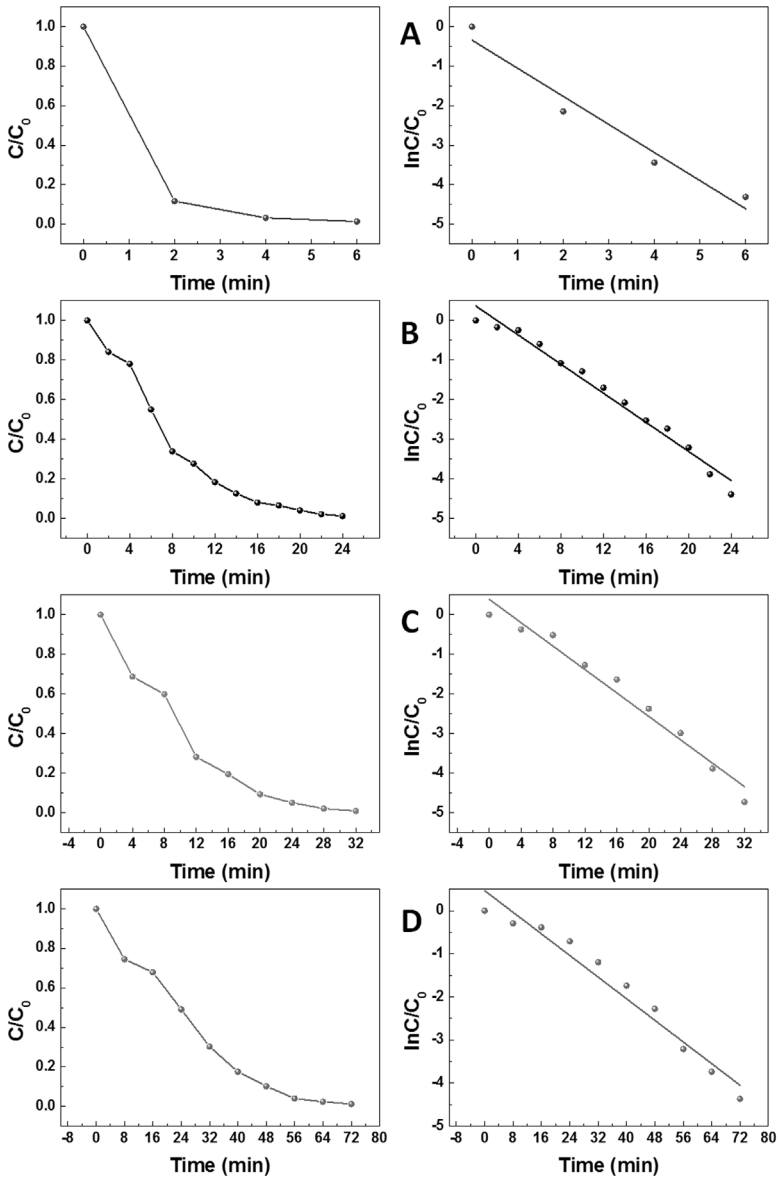

Figure 6. The hydrogenation reduction of *p*-NP with different concentrations of Ag/G. (A) Ag/G-s1, (B) Ag/G-s2, (C) Ag/G-s3, and (D) Ag/G-s4.

Hydrogenation Reduction of *p*-NP to *p*-AP

For the hydrogenation reduction of *p*-NP, in a typical process, 2.5 mL of aqueous solution of $NaBH_4$ (0.04 mol/L) was firstly added to 10 mL aqueous solution of *p*-NP (0.1 mmol/L). Afterwards, 1.0 mL Ag/G solution with different concentrations (i.e. 0.625, 0.156, 0.078, and 0.039 $mg \cdot mL^{-1}$, denoted as Ag/G-s1, Ag/G-s2, Ag/G-s3, and Ag/G-s4, respectively) were added to the mixed solution to start the reaction at 25 °C. The reduction process was monitored by measuring the absorption spectra with a UV-vis spectrophotometer (JASCO V–670 EX, Japan). To investigate the effect of reaction temperature on the reduction reaction, the *p*-NP reduction with Ag/G-s4 as the catalyst at 40 °C, 50 °C, and 60 °C were also investigated. For the exploration of the durability of the catalyst, the *p*-NP reduction with Ag/G-s2 as the catalyst was scaled up 10-fold. After reaction, the catalyst was recovered and reused by keeping all other parameters constant. For comparison, rGO and pure Ag nanoparticles were also tested for the reduction reaction. The dosage of rGO or Ag nanoparticles was measured according to the TGA result of Ag/G. The concentration of rGO or Ag nanoparticles was determined according to Ag/G-s2. The reaction process was also monitored by measuring the absorption spectra with the UV-vis spectrophotometer.

RESULTS AND DISCUSSION

Formation and Characterization of Ag/G Nanocomposites

GO has abundant oxygen-containing groups (e.g. epoxy, hydroxyl, and carboxyl groups), which endow the GO surface with negative charge. During the preparation process, Ag^+ can

Table 1. Reaction results of the hydrogenation reduction of *p*-NP with different concentrations of Ag/G

Catalyst	Concentrations (mg/mL)	Rate constants *k* (min^{-1})
Ag/G-s1	0.625	0.7112
Ag/G-s2	0.156	0.1837
Ag/G-s3	0.078	0.1479
Ag/G-s4	0.039	0.0627

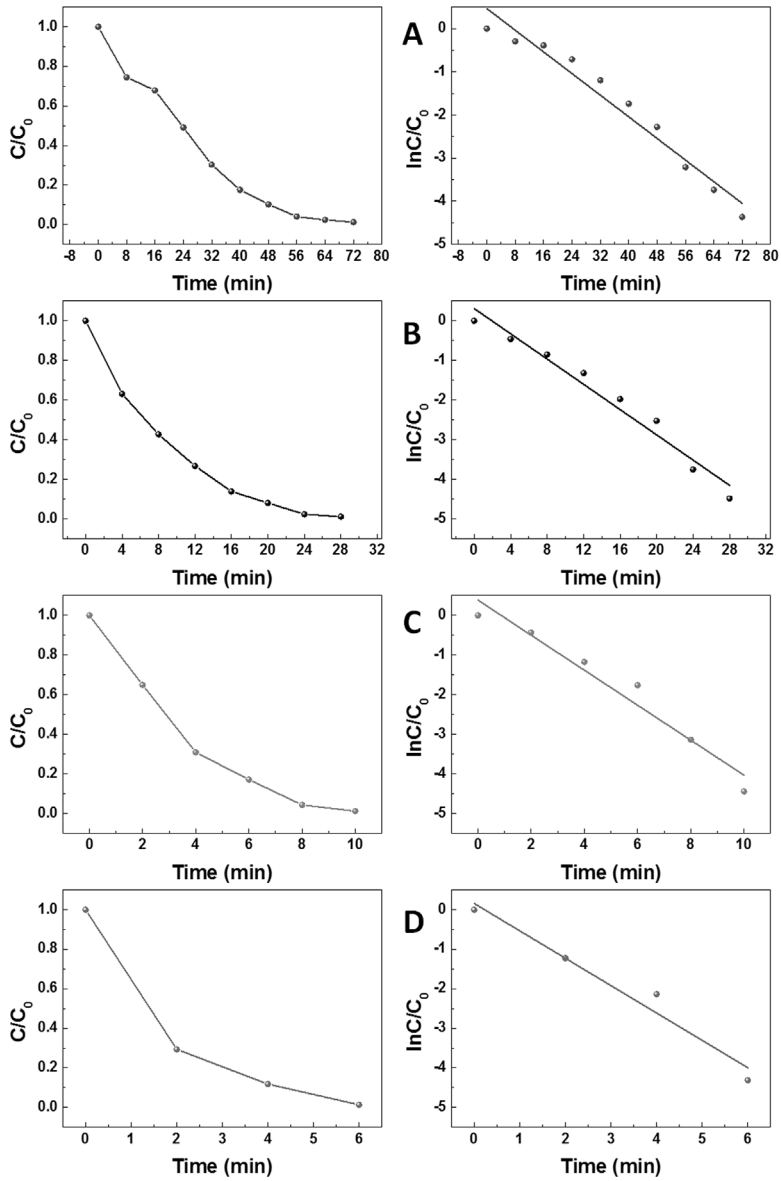

Figure 7. The hydrogenation reduction of *p*-NP at various temperatures with Ag/G-s4 as the catalyst. (A) 298 K, (B) 313 K, (C) 323 K, and (D) 333 K.

spontaneously interact with GO due to the electrostatic attraction. Moreover, in the presence of DMAc as reductant, the functional groups of GO act as nucleation sites for the formation and attachment of Ag nanoparticles, with a concomitant reduction of GO into rGO. The newly-formed Ag nanoparticles could bind to the surface of graphene (i.e. rGO) through dispersion and charge-transfer interactions, and Ag/G nanocomposites were thus obtained (Figure 1a). Figures 1b and 1c show the SEM images of rGO and Ag/G, respectively. The pure rGO sheets without Ag nanoparticles present a typical wrinkled and layered structure (Figure 1b), while Ag nanoparticles were uniformly wrapped into the rGO sheets in the Ag/G nanocomposites (Figure 1c). The mass percentage of Ag in the Ag/G composites was measured to be 0.814 g/g according the TGA results. The TEM image of Ag/G in Figure 1d showed that the Ag nanoparticles are homogeneously and densely attached to the graphene sheets. From the high-resolution TEM image (Figure 1e), the interplanar spacing with the graphene supported Ag nanoparticles is measured to be 0.23 nm, corresponding to the (111) lattice plane of Ag. The particle size distribution (PSD) of Ag nanoparticles obtained from the TEM image of Ag/G showed a narrow distribution within 10–35 nm, and the average particle size of Ag nanoparticles was 23.9 nm.

The binding of GO with Ag nanoparticles can also be monitored by UV-vis spectral analysis. As shown in Figure 2a, GO showed an absorption peak centred at 230 nm and a shoulder peak around 300 nm, which can be ascribed to the $\pi \rightarrow \pi^*$ transitions of aromatic C-C bonds and the $n \rightarrow \pi^*$ transitions of C=O bonds, respectively.[28–30] The rGO exhibited a shifted peak at about 265 nm, suggesting the deoxygenation of the GO after the reduction processes.[31] After decoration of Ag nanoparticles on the surface of graphene sheets, a new absorption peak at about 412 nm appeared, which is characteristic of Ag nanoparticles due to the surface plasmon absorption, indicating the formation of Ag/G. The XRD patterns in Figure 2b also confirmed the formation of Ag/G. The diffraction peaks at 37.8°, 44.0°, 64.2°, and 77.2° can be assigned to the (111), (200), (220), and (311) lattice planes of Ag, respectively.

Table 2. Reaction results of the hydrogenation reduction of *p*-NP at various temperatures with Ag/G (0.039 mg/mL) as the catalyst

T (K)	1000/T (K^{-1})	k (min^{-1})	Ln k
298	3.354	0.0627	−2.769
313	3.193	0.1594	−1.836
323	3.095	0.4416	−0.817
333	3.002	0.6925	−0.367

The diffraction peaks of GO at 10.6° and 42.3° disappeared upon the formation of Ag/G, indicating that GO has been reduced into rGO. According to the Scherrer equation, the Ag particle size calculated from the (111) peak of the XRD pattern of Ag/G is about 32.8 nm, which is comparable to the result obtained from the PSD analysis.

Hydrogenation Reduction of *p*-Nitrophenol to *p*-Aminophenol

The liquid-phase hydrogenation reduction of *p*-NP to *p*-AP in the presence of excess $NaBH_4$ was carried out to assess the catalytic performance of the materials. As shown in Figure 3a, the aqueous solution of *p*-NP shows an absorption peak at 317 nm. Upon the addition of $NaBH_4$, the absorption peak of the solution shifts to 400 nm, indicating the formation of *p*-nitrophenolate. Since the reduction of *p*-NP to *p*-AP with $NaBH_4$ is thermodynamically feasible but kinetically hindered by a high energy barrier,[32] the reaction of *p*-NP with $NaBH_4$ was hardly proceeding without the use of catalyst. The results in Figure 3b show that the absorbance spectra of mixture of *p*-NP and $NaBH_4$ did not change even after 2 h. By adding Ag/G nanocomposites (0.078 mg · mL^{-1}) as the catalyst, the absorption peak at 400 nm gradually decreased as the reduction reaction proceeded (Figure 3a). At the same time, a new adsorption peak at 297 nm, attributable to *p*-AP, appeared and progressively increased in intensity. After 24 min, the *p*-nitrophenolate ion peak disappeared (Figure 3a), indicating that the hydrogenation reduction reaction had proceeded completely to convert all *p*-NP into *p*-AP. In addition, it should be noted that the isosbestic point at 313 nm suggests that no side reaction took place with *p*-AP as the only product.[33] No morphology change of Ag/G-s2 can be observed after the reduction reaction (Figure 4). For comparison, the performance of pure Ag nanoparticles for the catalytic reaction of *p*-NP to *p*-AP was also tested. It can be observed that the reaction rate was significantly slower than that of Ag/G, which can be attributed to the severe agglomeration of Ag nanoparticles. The hydrogenation reduction of *p*-NP in the presence of excess $NaBH_4$ follows the Langmuir-Hinshelwood model,[34] in which pseudo-first-order kinetics can be applied for the evaluation of the catalytic rate. Therefore, the kinetic equation for the reaction can be illustrated as the following:

$$\ln\left(\frac{C}{C_0}\right) = -kt \tag{1}$$

where C_0 and C are the initial concentration of *p*-NP and the concentration of *p*-NP at time t, respectively. C/C_0 can be measured from the relative peak intensity at 400 nm in the UV-vis optical spectra, as presented in Figure 3c, and Figure 3d shows the linear relationship of $\ln(C/C_0)$ versus reaction time. A plot of $\ln(C/C_0)$ versus t can yield the apparent rate constant k for the reduction of *p*-NP from the slope of the curve fitting line. The apparent rate constants were calculated to be 0.1837 min^{-1} and 0.0226 min^{-1} for Ag/G and Ag nanoparticles, respectively. Based on the unique properties of Ag and graphene, the reaction mechanism with Ag/G as the catalyst for the hydrogenation reduction of *p*-NP can be speculated in the present study. As shown in Figure 5, the electrons injected from BH_4^- can form an electron-enriched region[35] on the surface of the Ag nanoparticles supported by graphene, which facilitates the uptake of electrons by the *p*-NP molecules. Therefore, the *p*-NP adsorbed on graphene can be readily reduced into *p*-AP, and then the *p*-AP molecules desorb into the solution. In addition, the high adsorption capability and extraordinary electronic transport property of graphene further make it an excellent reaction platform for the reduction reaction, as observed in this study.

Effects of Catalyst Concentrations on the Reaction

The hydrogenation reduction of *p*-NP with various concentrations of Ag/G samples were also investigated, and the reaction results are shown in Figure 6 and Table 1. It can be observed that the reaction becomes faster with increasing of the concentration of Ag/G. With Ag/G-s1 (0.625 mg/mL) as the catalyst, the reaction can be completed in only 6 min. Further increasing of the concentration of Ag/G will make the reaction too fast to track. These comparison results suggest the high efficiency of Ag/G as the catalyst for the hydrogenation reduction of *p*-NP.

Effects of Temperatures on the Reaction

The catalytic reduction of *p*-NP with Ag/G (0.039 mg/mL) as the catalyst was further carried out at various temperatures, and the results are shown in Figure 7 and Table 2. It can be observed that higher temperature induced faster kinetics for the reduction reaction, with the rate constants at different temperatures listed in Table 2.

The apparent activation energy (Ea) can be measured from the Arrhenius equation:

$$\ln k = -\frac{Ea}{R}\cdot\frac{1}{T} + \ln A \tag{2}$$

where k is the apparent rate constant, T is the temperature, R is the molar gas constant, and A is the pre-exponential factor. Figure 8

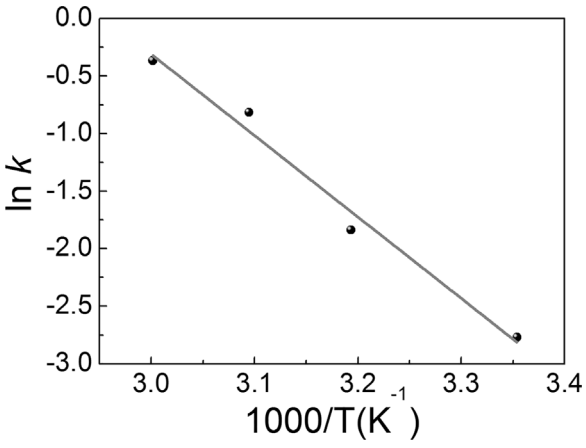

Figure 8. Arrhenius plot for the reduction reaction of *p*-NP with Ag/G as the catalyst at various temperatures.

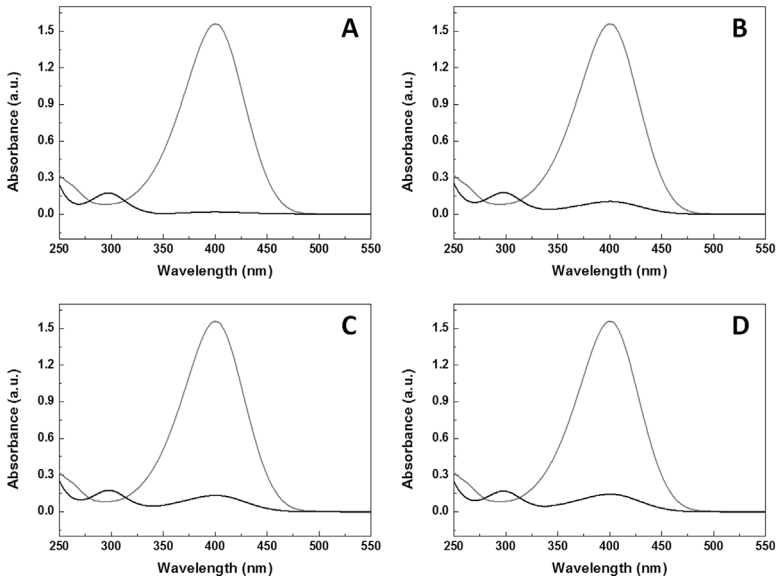

Figure 9. The reduction of *p*-NP with Ag/G-s2 as the catalyst for the repeated use of four times. (A) First use, (B) second use, (C) third use, and (D) fourth use.

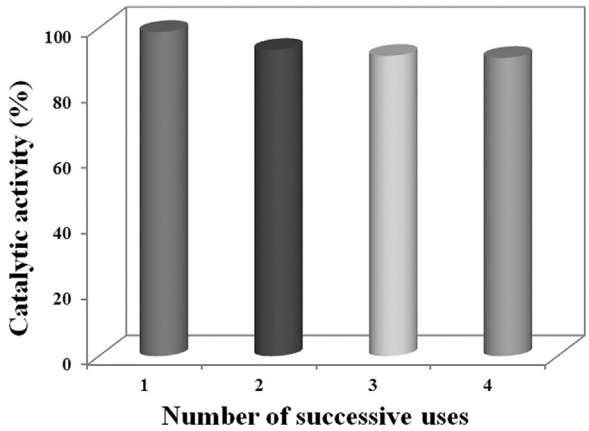

Figure 10. Evaluation of the durability of Ag/G as the catalyst for the hydrogenation reduction of *p*-NP within four cycles.

shows the linear fitting of ln k versus 1000/T. And the apparent activation energy was calculated to be 58.8 kJ/mol.

Durability Studies of the Ag/G Catalysts

The durability of the Ag/G as catalyst for the hydrogenation reduction of *p*-NP was also investigated (Figure 9). It can be observed that the catalytic stability can be well reserved after 4 cycles (Figure 10), with no obvious decrease detected on the catalytic activity for the repeated use during four times. These results demonstrate that Ag/G is a very efficient and stable catalyst for hydrogenation reduction of *p*-NP.

CONCLUSIONS

In conclusion, we have demonstrated that one-step and stabilizer-free synthesized Ag/G can act as an efficient catalyst for hydrogenation reduction of *p*-NP. The reaction kinetics of the catalytic reduction, including the effects of catalyst concentrations and temperatures, have been systematically investigated. These results are of significant value for the scale-up of using Ag/G catalysts for hydrogenation reduction.

ACKNOWLEDGEMENTS

This work is partially supported by National Natural Science Foundation of China (51641201, 21622601, and 201620102007), National Key R&D Program of China (2016YFA0201701/2016YFA0201700), and the Fundamental Research Funds for the Central Universities (BUCTRC201601, JD1606). Dr. Jiangyong Liu is also grateful to the High-Level Talents Research Fund of Yangzhou University.

REFERENCES

[1] Y. Du, H. Chen, R. Chen, N. Xu, *Appl. Catal. A-Gen.* **2004**, *277*, 259.

[2] S. Saha, A. Pal, S. Kundu, S. Basu, T. Pal, *Langmuir* **2010**, *26*, 2885.

[3] K.-L. Wu, X.-W. Wei, X.-M. Zhou, D.-H. Wu, X.-W. Liu, Y. Ye, Q. Wang, *J. Phys. Chem. C* **2011**, *115*, 16268.

[4] S. Wu, J. Dzubiella, J. Kaiser, M. Drechsler, X. Guo, M. Ballauff, Y. Lu, *Angew. Chem. Int. Edit.* **2012**, *51*, 2229.

[5] P. Pachfule, S. Kandambeth, D. D. Díaz, R. Banerjee, *Chem. Commun.* **2014**, *50*, 3169.

[6] X. Guo, Q. Zhang, Y. Sun, Q. Zhao, J. Yang, *ACS Nano* **2012**, *6*, 1165.

[7] Y. Khalavka, J. Becker, C. Sonnichsen, *J. Am. Chem. Soc.* **2009**, *131*, 1871.

[8] J. A. Johnson, J. J. Makis, K. A. Marvin, S. E. Rodenbusch, K. J. Stevenson, *J. Phys. Chem. C* **2013**, *117*, 22644.

[9] B. Baruah, G. J. Gabriel, M. J. Akbashev, M. E. Booher, *Langmuir* **2013**, *29*, 4225.

[10] J. Wang, X.-B. Zhang, Z.-L. Wang, L.-M. Wang, W. Xing, X. Liu, *Nanoscale* **2012**, *4*, 1549.

[11] J. Zhang, G. Chen, D. Guay, M. Chaker, D. Ma, *Nanoscale* **2014**, *6*, 2125.

[12] S. Gu, Y. Lu, J. Kaiser, M. Albrecht, M. Ballauff, *Phys. Chem. Chem. Phys.* **2015**. *17*, 28137.

[13] Y.-Y. Shen, Y. Sun, L.-N. Zhou, Y.-J. Li, E. S. Yeung, *J. Mater. Chem. A* **2014**, *2*, 2977.

[14] S. Hemidouche, L. Boudriche, A. Boudjemaa, S. Hamoudi, *Can. J. Chem. Eng*. **2017**, *95*, 508.

[15] A. Davies, A. Yu, *Can. J. Chem. Eng*. **2011**, *89*, 1342.

[16] Y. Hao, Z. Wang, J. Gou, Z. Wang, *Can. J. Chem. Eng*. **2015**, *93*, 1713.

[17] S. Guo, S. Dong, E. Wang, *ACS Nano* **2009**, *4*, 547.

[18] Y. Liang, Y. Li, H. Wang, J. Zhou, J. Wang, T. Regier, H. Dai, *Nat. Mater*. **2011**, *10*, 780.

[19] G. Gao, H. B. Wu, X. W. D. Lou, *Adv. Energy Mater*. **2014**, *4*, 1400422.

[20] C. Hu, Y. Liu, J. Qin, G. Nie, B. Lei, Y. Xiao, M. Zheng, J. Rong, *ACS Applied Materials and Interfaces* **2013**, *5*, 4760.

[21] Z. Zhang, F. Xu, W. Yang, M. Guo, X. Wang, B. Zhang, J. Tang, *Chem. Commun*. **2011**, *47*, 6440.

[22] Z. Fan, B. Liu, J. Wang, S. Zhang, Q. Lin, P. Gong, L. Ma, S. Yang, *Adv. Funct. Mater*. **2014**, *24*, 3933.

[23] L. Xu, G. Yang, H. Jing, J. Wei, Y. Han, *Nanotechnology* **2014**, *25*, 055201.

[24] H. Zhao, J. Song, X. Song, Z. Yan, H. Zeng, *J. Mater. Chem. A* **2015**, *3*, 6679.

[25] W. S. Hummers Jr., R. E. Offeman, *J. Am. Chem. Soc*. **1958**, *80*, 1339.

[26] J. Qian, D. Wang, F. Cai, W. Xi, L. Peng, Z. Zhu, H. He, M. Hu, S. He, *Angew. Chem. Int. Edit*. **2012**, *51*, 10570.

[27] C. Ran, M. Wang, W. Gao, Z. Yang, J. Deng, J. Ding, X. Song, *Phys. Chem. Chem. Phys*. **2014**, *16*, 4561.

[28] D. Wang, L. Zhu, J.-F. Chen, L. Dai, *Nanoscale* **2015**, *7*, 9894.

[29] D. Wang, J. Liu, J.-F. Chen, L. Dai, *Advanced Materials Interfaces* **2016**, *3*(1), 1500439.

[30] D. Wang, L. Zhu, C. McCleese, C. Bruda, J.-F. Chen, L. Dai, *RSC Adv*. **2016**, *6*, 41516.

[31] O. Akhavan, E. Ghaderi, S. Aghayee, Y. Fereydooni, A. Talebi, *J. Mater. Chem*. **2012**, *22*, 13773.

[32] L. Guardia, J. I. Paredes, J. M. Munuera, S. Villar-Rodil, M. Ayán-Varela, A. Martínez-Alonso, J. M. Tascón, *ACS Applied Materials and Interfaces* **2014**, *6*, 21702.

[33] S. Gu, S. Wunder, Y. Lu, M. Ballauff, R. Fenger, K. Rademann, B. Jaquet, A. Zaccone, *J. Phys. Chem. C* **2014**, *118*, 18618.

[34] H. Zhang, X. Li, G. Chen, *J. Mater. Chem*. **2009**, *19*, 8223.

[35] P. Herves, M. Pérez-Lorenzo, L. M. Liz-Marzán, J. Dzubiella, Y. Lu, M. Ballauff, *Chem. Soc. Rev*. **2012**, *41*, 5577.

Manuscript received November 10, 2016; revised manuscript received December 2, 2016; accepted for publication December 5, 2016.